Int J Adv Manuf Technol (2016) 86:989–998
DOI 10.1007/s00170-015-8210-z

ORIGINAL ARTICLE

A study of cutting factors affecting the generation of functional hierarchical rib array structure in ultra-precision raster milling

H. T. Wang[1] · **W. B. Lee**[1]

Received: 10 June 2015 / Accepted: 7 December 2015 / Published online: 30 December 2015

Abstract Hierarchical ribs can be used to keep balance between heat transfer enhancement and pressure drop reduction. The unique hierarchical structure which features a first-order asymmetric arc rib imposed by second-order microgrooves greatly reduces the pressure drop as well as enhances the heat transfer. However, it is hard for conventional machining techniques to generate such complicated configurations, especially freeform geometries in the micron range. Taking advantage of ultra-precision raster milling (UPRM), a novel one-step machining process, for advanced hierarchical ribs is proposed and demonstrated. In this paper, the principle of the cutting strategy for the second-order microstructures and cutting conditions that affect the basic features of the structures are discussed. In addition, three-level factorial design of cutting speeds, feed rates, and depth of cuts were set and used to machine hierarchical ribs on a copper workpiece. It was found that the cutting strategy was affecting the geometry of second-order microstructures of hierarchical ribs in UPRM. Moreover, the result revealed that at low levels of feed rate and cutting depth, a middle level of cutting speed provides a better quality of second-order microstructures than a middle level of feed rate, high level of cutting depth, and low level and high level of cutting speed. Maintaining a balance between machining efficiency and hierarchical structure generation quality is thoroughly assessed by machining second-order microgrooves on asymmetric arc primary surfaces.

✉ W. B. Lee
wb.lee@inet.polyu.edu.hk

[1] State Key Laboratory in Ultra-precision Machining Technology, Department of Industrial and Systems Engineering, The Hong Kong Polytechnic University, Hung Hom, Kowloon, Hong Kong, SAR, China

Keywords Hierarchical rib · One-step machining · Ultra-precision raster milling · Cutting strategy · Cutting conditions

1 Introduction

Artificial roughness has been investigated for a few decades for their special function in enhancing heat transfer in heat exchangers [1–3]. It is found that the transverse ribbed surface in cooling channels could enhance heat transfer rates by forced convection. Several investigators have verified this phenomenon through simulations and experiments [4–7]. The ribbed surfaces act as a turbulence generator to break down the thermal resistance layer near the surface, therefore enhancing the heat transfer. However, with the improvement of heat transfer, the pressure drop will greatly increase. In order to keep a balance between enhancing heat transfer and minimizing pressure drop, a more complex hierarchical rib is employed by the authors [8]. Compared to other shaped ribs, hierarchical ribs with asymmetric arc geometry could avoid generating the fore eddy as well as promote the separated flow to reattach the surface. A typical cooling channel and the practical surface topography of a hierarchical rib are illustrated in Fig. 1. Flow direction is from right to left in the graphs indicated by the pointed arrow. Based on the flow boundary condition, the dimensions and arrangement of ribs need to be adjusted.

Different machining techniques have been attempted to fabricate these microstructures on cooling surface. The conventional methods commonly used include laser beam machining [9], grinding [10], wire electrochemical machining [11], ploughing extrusion [12], etc. However, conventional machining techniques cannot deal with more complex configurations, such as freeform

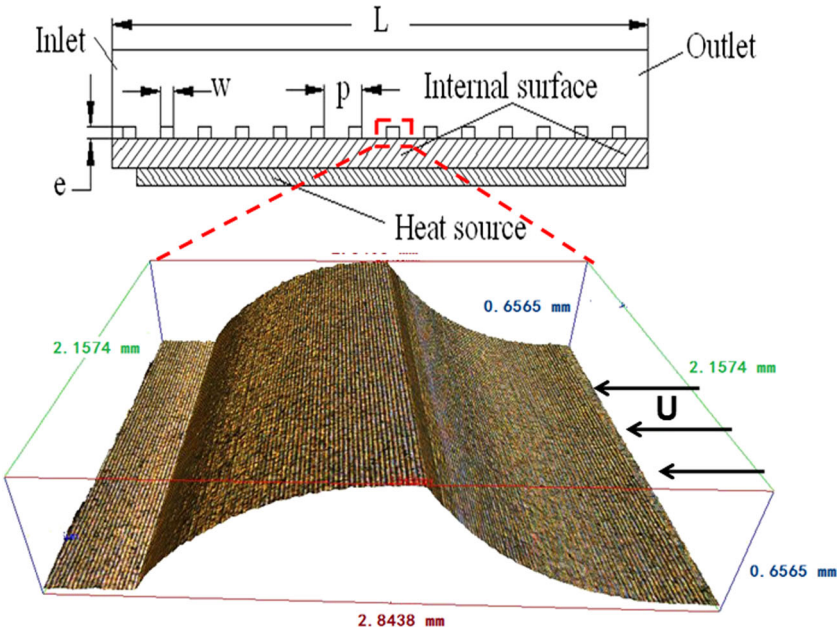

Fig. 1 The scheme of single-phase channel with various shapes of microstructures for heat exchange. **a** The dimensions of the channel and microstructure and **b** the enlarge freeform ribs withrib height e=600 μm and the width of rib to the height of rib w/e=4

geometries in the micron range. Ultra-precision raster milling (UPRM) is an ultra-precision machining technology making use of a single crystal diamond tool for fabricating non-rotational freeform surfaces with nanometric surface roughness and sub-micrometric form accuracy, without the need for any subsequent post-polishing [13].

Cutting conditions and cutting strategies play an important role in machining components' surface quality, which have been studied by employing theoretical and experimental techniques to provide the optimum feed and speed [14–16]. Kong et al. [17] conducted a series of experiments to study the effect of different cutting factors on surface generation in ultra-precision raster milling. It was found that the surface roughness is critically influenced by the machining factors (i.e., tool geometry, cutting strategy, and tool wear), and the form accuracy of freeform surfaces is greatly affected by machining tool characteristics (i.e., slide motion errors, spindle error motions, and the relative vibration between the tool and the workpiece). Cheng et al. [18] built a simulation system to predict the surface generation precision and optimize cutting conditions and cutting strategy in ultra-precision raster milling. Duong et al. [19] introduced a prediction method for the deformation of the microchannels in the ultra-precision machining process.

A dynamic model was established by Zhang and To [20], which was employed to study the impact of cutting force on surface generation under spindle vibration in ultra-precision raster milling. Albertelli et al. [21] used simplified models to analyze the effect of machine on spindle dynamics. It was found that the stability of the cutting process can be enhanced by controlling tuning criteria. In order to improve the quality of surface in a given machining time, Wang et al. [22] reported a new methodology to integrate the optimization of cutting conditions and tool path generation by the prediction models for ultra-precision raster milling. Gao et al. [23]) proposed a reverse calculation method to predict the form errors and evaluate the capacity of ultra-precision machining.

The previous research works have studied different methods and techniques to optimize the machining parameters and strategies for ultra-precision milling operations to generate a lower roughness plane or various freeforms. There is a lack of investigation in regard to the optimization of hierarchical microstructure generation in ultra-precision raster milling. Moreover, accompanied with high-accuracy surface roughness and low form error, ultra-precision raster milling usually consumes considerable time and cost because of the trial-and-error cutting approaches. Maintaining a balance between efficiency and accuracy of surface generation is important. In this research, UPRM was used to generate hierarchical asymmetric rib in a one-step machining process. A series of cutting experiments was carried out to study the effect of different factors and cutting strategy on the quality of hierarchical ribs and the efficiency of machining process.

2 Experimental

2.1 Hardware configuration of the experiment

After machining, the samples were cleaned. Since the thermal and dynamic performance of 2D transverse ribs is very sensitive to the quality of configurations and arrangements of ribs,

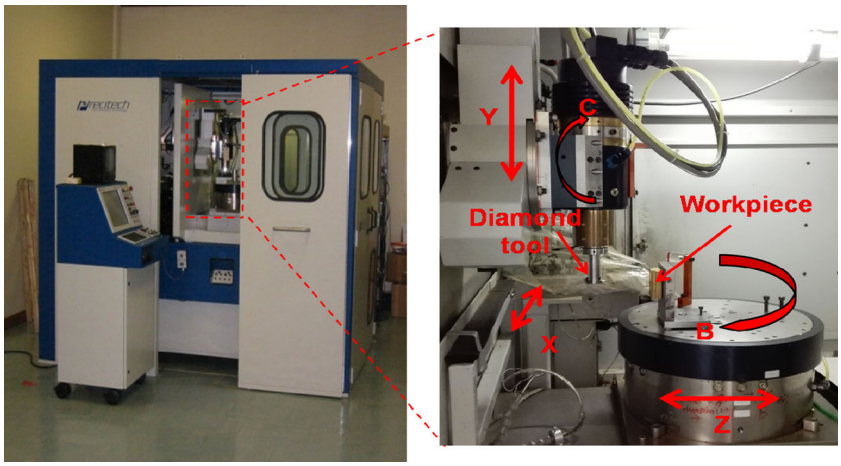

Fig. 2 Freeform 705G ultra-precision machine and five axes of machine tool

UPRM was performed on a Freeform 705G (Precitech Inc., USA), which is shown in Fig. 2. UPRM provides a solution for machining freeform surfaces with sub-micrometric form accuracy and nano-metric surface roughness without the need for any subsequent post-polishing.

The specifications for linear axis and spindle motion of the machine are shown in Fig. 2. The diamond tool is attached to the spindle. The workpiece is clamped on the fixture and follows the linear motion along the *Y*-axis and rotational motion. The machine performs high precision feed for 3D milling, grinding, and two-axis turning. For the Freeform 705G machine, there are three linear axis (*X, Y, Z*) movements and two rotational axis (B, C) movements.

2.2 Cutting strategy

There are two possible cutting strategies: One is horizontal cutting and the other is vertical cutting, as shown in Figs. 3 and 4, respectively. There are two main motions during the cutting process: the feed motion and the raster motion. According to the characteristics of the desired surface topology and the geometry of the functional ribs, different appropriate cutting strategies are required in UPRM. The horizontal cutting strategy is shown in Fig. 3, in which the cutting tool feed direction is horizontal. After finishing one cutting step, the diamond tool moves a step in the raster direction. The process is repeated over the whole surface. Figure 4 shows the vertical cutting strategy, in which the feed direction is along the vertical direction, while the diamond tool moves a step in the horizontal direction.

The principle of the generation of the hierarchical microstructures by horizontal cutting strategy is shown in Fig. 3. The diamond tool is fixed to the main spindle and forms a cutting plane when the spindle rotates. Figure 3a shows the tool path of machining the primary structure on the material surface under horizontal cutting strategy. Because the feed direction is parallel to the transverse rib, after the diamond tool cuts the surface, a series of second-order microgrooves, along the transverse direction, was generated on the rib surface. The depth of microgroove was determined by the step distance and tool angle. The generation of second-order microgrooves is shown in Fig. 3b. The red characters (i.e., $T_1, T_2 \ldots T_n$) represent the order of the cutting steps with a given constant cutting depth of ε, and the subscript n is the number of cutting times to generate a desired depth of groove. For example, if the cutting depth is ε=2μm, it needs to cut n=10 times to obtain a groove with the desired depth d of 20 μm.

For horizontal cutting, based on the relationship of step distance w, desired microgroove distance d, and cutting tool angle α, the ideal depth of microgrooves can be calculated by

$$d = \frac{1}{2} w \cdot ctg\left(\frac{\alpha}{2}\right) \tag{1}$$

where d is the desired depth, w is the step distance, and α is the cutting tool angle.

The machining process of the vertical cutting strategy is shown in Fig. 4. Due to the feed direction being parallel to the transverse rib, after the diamond tool cuts the surface, a series of tool interval marks, which cross the transverse direction, was generated on the rib surface. The tool path of vertical cutting strategy is shown in Fig. 4a; the calculation model of the artificial roughness is shown in Fig. 4b; the scallop of tool interference in the depth direction is calculated by

$$h = \sqrt{R^2 - \left(\frac{\omega}{2}\right)^2} \tag{2}$$

When the spindle of the machine rotates at a given speed ω, the flying diamond tool traces a circular plane. The radius of the circle equals to the swing distance R.

2.3 Tool path

According to the relative position of the flying tool plane and the ribs, there are two types of machining method to control the

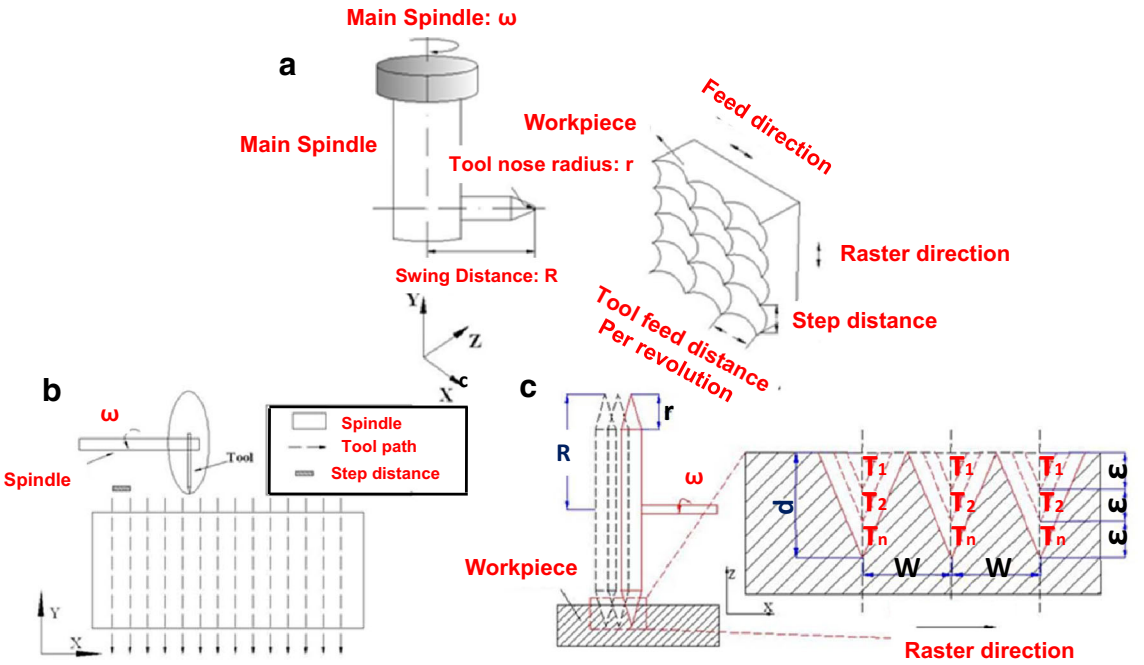

Fig. 3 The horizontal cutting strategy: **a** relative position of cutting tool and workpiece, **b** tool path (*top view*), and **c** ideal artificial roughness profiles and mechanism of forming microgrooves (*side view*)

microtexture on the rib surface as shown in Fig. 4. The dimensions of transverse ribs are much smaller than the swing radius value of *R*. If the flying tool plane is in the *Y*–*Z* coordinate plane (parallel to the longitudinal direction), the interference between the diamond tool and transverse ribs will occur as shown in Fig. 5a. When the flying tool plane machines the microstructures in the *X*–*Z* plane, the interference could be avoided as shown in Fig. 5b

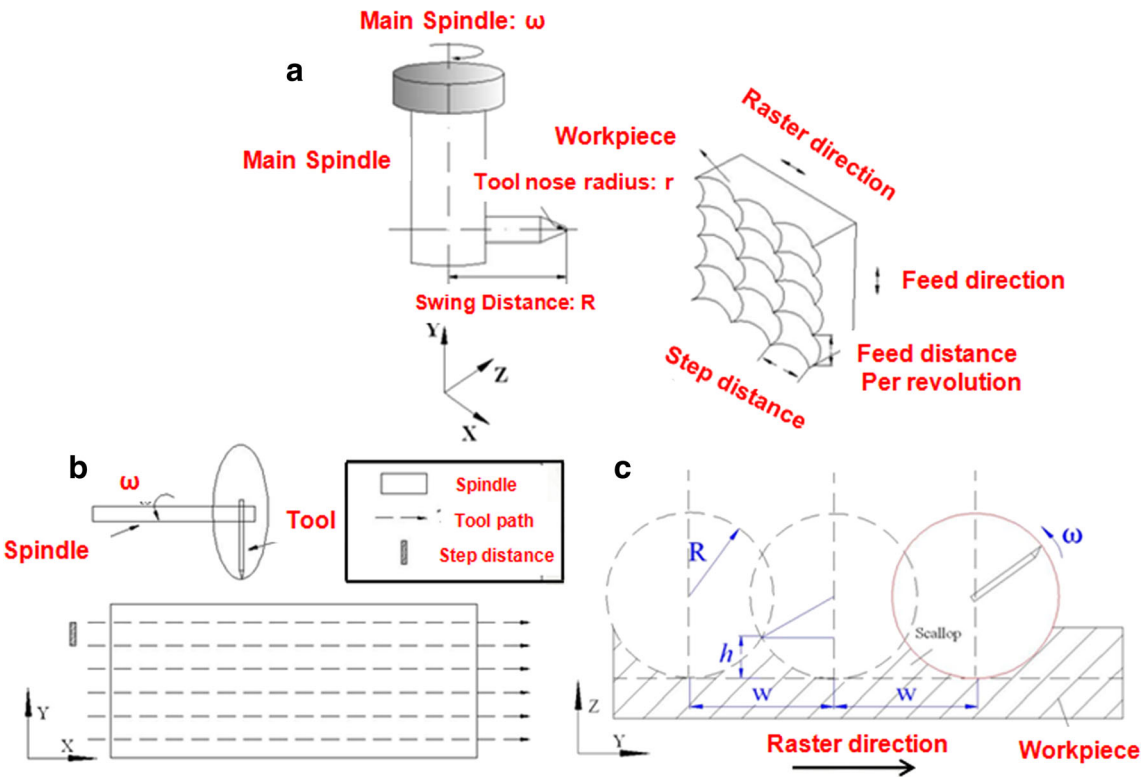

Fig. 4 The vertical cutting strategy: **a** relative position of cutting tool and workpiece, **b** tool path (*top view*), and **c** ideal artificial roughness profiles (*side view*)

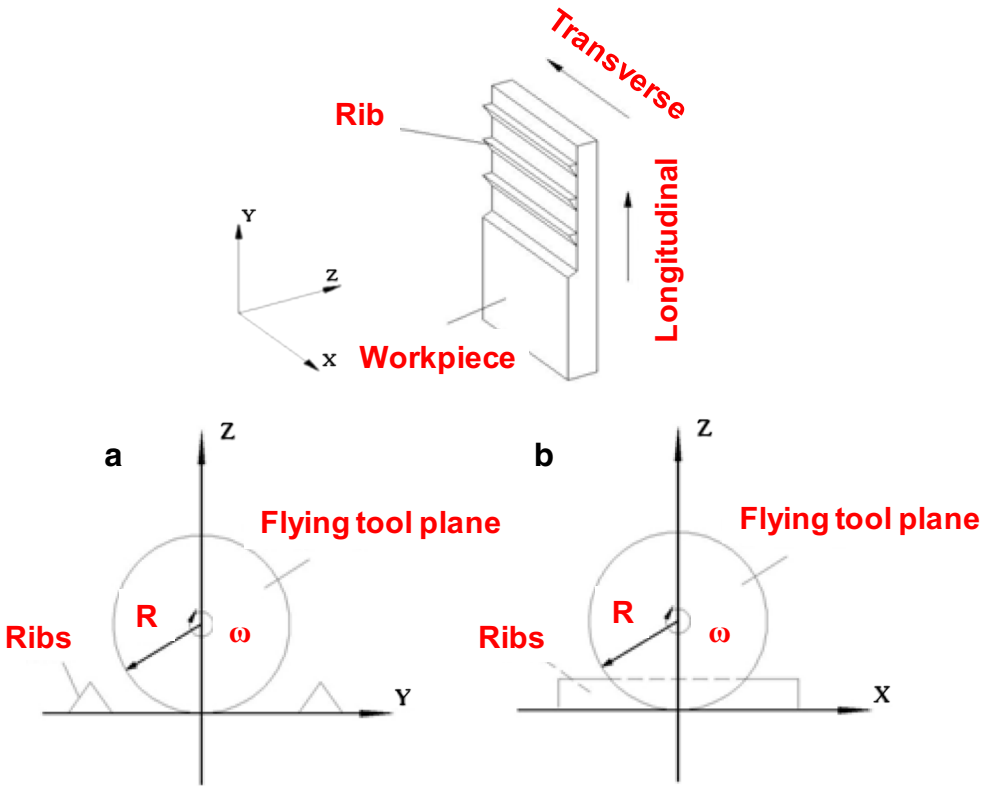

Fig. 5 The relative position of workpiece and flying cutting tool plane: **a** tool plane in *Y–Z* plane and **b** tool plane in *X–Z* plane

2.4 Cutting parameter determinations

The diamond tool plays a very important role in the one-step machining process, and the shape of the cutting tool determines the shape of second-order microgrooves.

Single crystal diamond tools have many outstanding advantages involving nano-metric edge sharpness, high reproducibility, and high wear resistance. A sharp tool whose radius of arc is extremely small is required to fabricate some special types of components, such as V-grooves. The sharp diamond tool with a 40° tool angle is shown in Fig. 6.

The machining parameters such as cutting depth, revolution speed of the spindle, feed rate, step distance, and cutting tool angle are the critical factors that affect the surface texture and form accuracy. Three groups of machining experiments were conducted (i.e., groups 1 to 3) to study the effect of the cutting conditions (i.e., cutting depth, revolution speed of the spindle, feed rate, and tool angle) on the second-order microstructure generation. The cutting conditions are shown in Table 1.

Hierarchical ribs are machined by horizontal cutting strategy, and the step distance determines the depth of second-order microgroove. In this study, the desired depth of second-order microgroove was set as d=20 μm. According to Eq. (1), in order to obtain the desired depth of microgroove, the step distance w was set as 8.68, 14.56, and 20 μm for tool angles of 25.5°, 40°, and 90°, respectively.

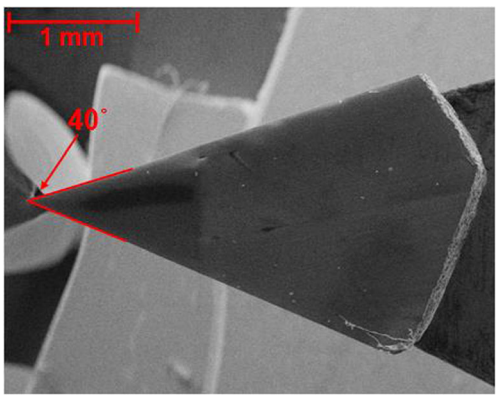

Fig. 6 The SEM photo of sharp diamond tool with tool 40° angle used in UPRM

3 Results and discussion

3.1 Effect of cutting strategy

The surface generation for different cutting strategies has been introduced in Sect. 2. Examples of the machined cross section of microstructures are given in Fig. 7. Asymmetric arc ribs with and without transverse second-order microstructures machined are shown in Fig. 7a, b, respectively.

In Fig. 7a, the second-order microgroove arrays overlap on the primary asymmetric rib surface. These surface features greatly contribute to the enhancement of the heat transfer rate and minimizing of the pressure drop in a microstructure heat exchanger.

Table 1 Set of cutting conditions in the machining experiments

Group Cutting condition	1 Cutting depth ε	2 Revolution speed of the spindle ω	3 Feed rate f
α (°)	25.5, 40, 90	25.5	25.5
ε (μm)	2, 5, 8	2	2
ω (rpm)	4000	2000, 4000, 6000	4000
f (mm/min)	50	50	50, 100, 150

Due to the flow speed of the viscous layer being very slow near the smooth surface, it will form a thermal resistance layer between the heat surface and high-flow speed upper layer. The second-order microgrooves contribute to break the thermal resistance layer and enhance the flow convection, thereby enhancing transfer of local heat to the upper layer. Moreover, the second-order microgrooves also act as a turbulence generator, which can reduce the weak region of the leeward side of ribs and minimize the form pressure.

The SEM micrograph of an asymmetric rib without transverse microgrooves is shown in Fig. 7b. The artificial roughness of the asymmetric arc rib is found to be relatively smaller than ribs machined by vertical cutting. In order to improve the efficiency of fabrication for the microstructures, increasing the step distance is one of the possible methods. However, the path-interval scallop height also increases with increasing step distance, which may influence the flow near the wall. Nikuradse [24]) classified the characteristics of the rough surface into three regimes, as follows:

1. Hydrodynamic smooth surface: $0<u_\tau\varepsilon/\nu\leq 5$,
2. Transition rough surface: $5<u_\tau\varepsilon/\nu\leq 70$,
3. Complete rough surface: $70<u_\tau\varepsilon/\nu$,

where u_τ is the friction velocity, $\tau_\omega=f\rho u^2/2$ is the shear stress, $f=0.046/Re^2$ is the fining friction factor, u is the average velocity, ρ is the fluid density at the wall, e is the equivalent roughness height, ν is the kinematics viscosity, and Re is the Reynolds number. According to the flow boundary conditions, the step distance should be controlled within a reasonable range, which ensures that the artificial roughness is a hydrodynamic smooth surface.

Figure 8 shows the topography of arc asymmetric rib surface machined by vertical cutting. It can be seen that the scallop direction is along the X-axis (longitudinal direction). The step distance is 240 μm, and the highest height of peak to valley is about 5 μm. For flow with a high Reynolds number (i.e., Re from 20,000 to 60,000), the artificial roughness surface could be considered as a hydrodynamic smooth surface, which means that the artificial roughness will not affect the flow near the wall at this scale.

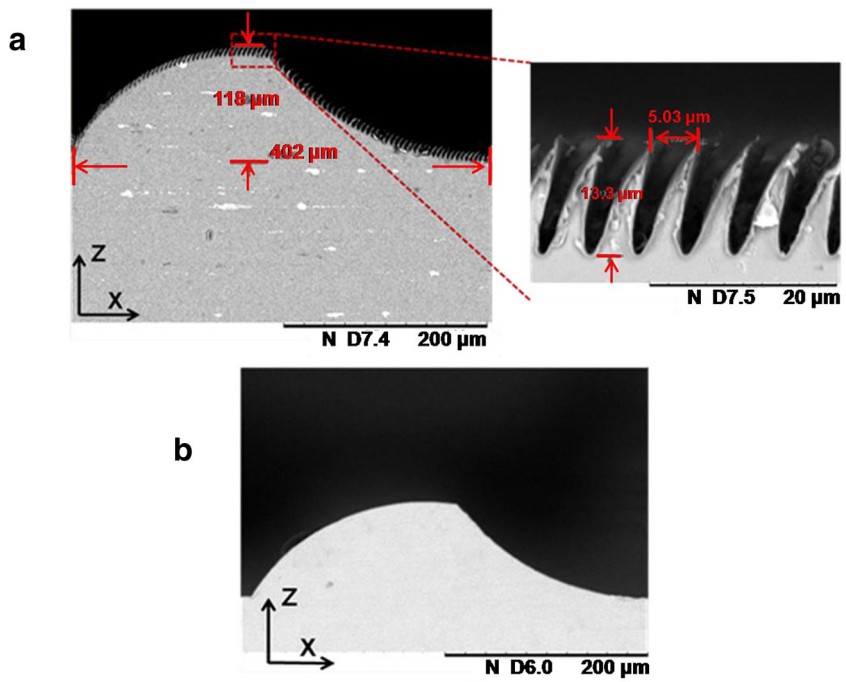

Fig. 7 SEM micrograph of cross section of a transverse rib **a** obtained by horizontal cutting strategy and **b** machined by vertical cutting strategy

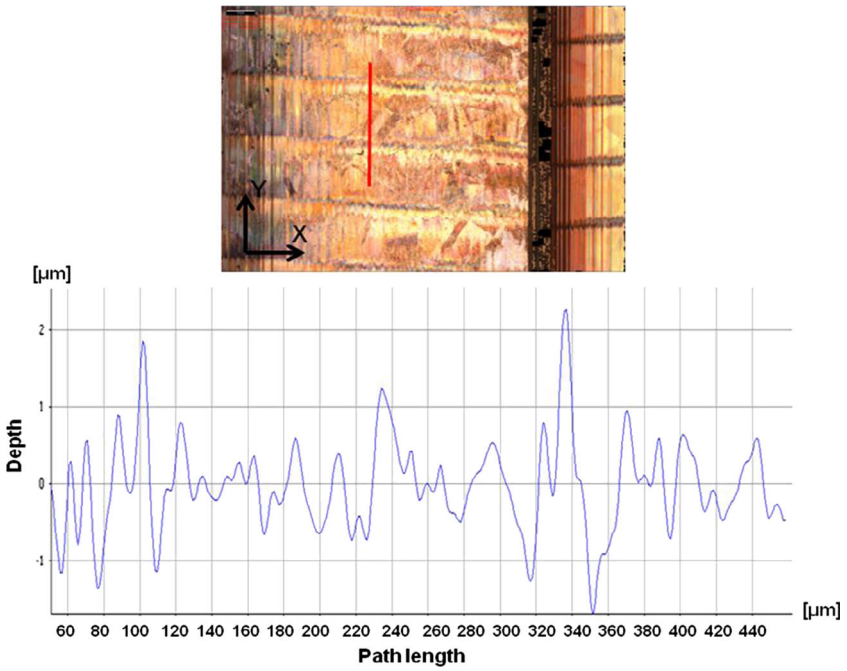

Fig. 8 Surface roughness of ribs machined by vertical cutting **a** topography of rib surface and **b** profile of surface roughness (measured by 3D optical measurement system)

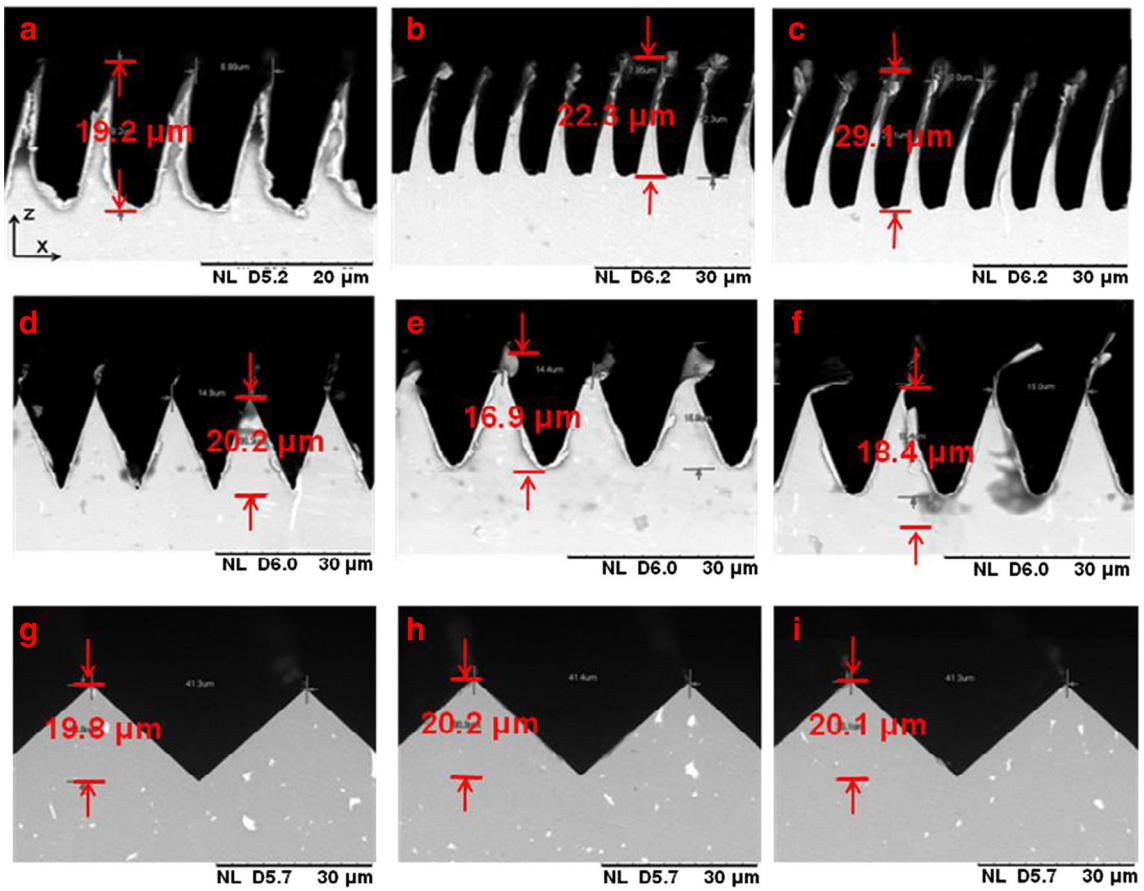

Fig. 9 The SEM microphotographs of cross-sectional second-order microgrooves machined by UPRM; the cutting depths are 2, 5, and 8 μm from left to right. **a**–**c** Machined by 25.5° tool angle, **d**–**f** machined by 40° tool, and **g**–**i** machined by 90° tool angle

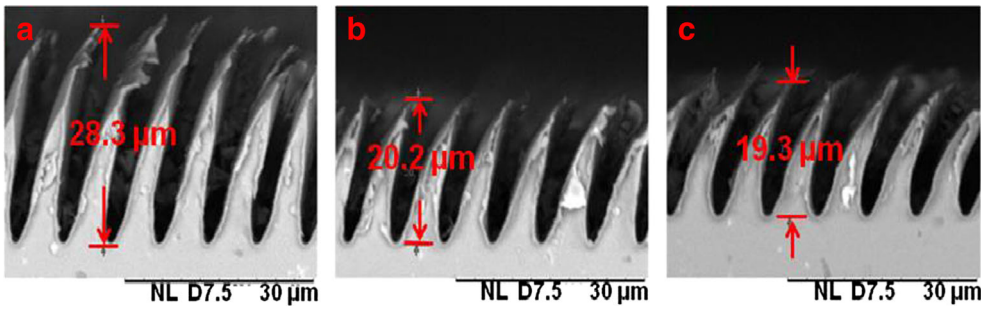

Fig. 10 The SEM of second-order microgrooves machined by UPRM at different revolution speed of spindles ω for tool angle 25.5°: **a** ω=2000 rpm, **b** ω=4000 rpm, and **c** ω=6000 rpm

3.2 The effect of cutting depth with different tool angles

The effect of cutting depth on the microgrooves was studied. The cutting experiments were carried out under group 1. The other cutting parameters were fixed. The revolution speed of the spindle was 4000 rpm, and the feed rate was 50 mm/min. Figure 9 shows the second-order microgrooves machined by different cutting depths of 2, 5, and 8 μm from left to right, respectively.

The second-order microgrooves machined by the 25.5° diamond tool are shown in Fig. 9a, b, c. It can be seen that the differences between the three testing groups of microgrooves are very obvious. Figure 9a shows the microgrooves machined by a 25.5° diamond tool at the cutting depth of 2 μm. The shape of the microgroove is a regular "V," and the top of the groove is very thin while the root is thick. The depth of the microgroove is 19.2 μm for a cutting depth of 2 μm, which is close to the desired depth of 20 μm. In addition, the top of the groove ridge bends slightly toward the opposite raster motion direction for the tool angle of 25.5°, but no such plastic distortion occurs on the roots of the grooves where the tooth of groove is relatively thicker. The microgrooves were machined by 40° and 90° and are shown in Fig. 9b, c. Due to the existence of burrs on the tops of the microgrooves, the depths are much deeper for the set values of the microgrooves under a cutting depth of 5 and 8 μm, and the measured depths of microgroove are 22.3 and 29.1 μm, respectively. So, the results show that the phenomenon of burrs becomes more serious with increasing depth of cut.

The microgrooves machined by the 40° diamond tool are shown in Fig. 9d, e, f under the cutting depths of 2, 5, and 8 μm, respectively. There still exists some burrs on the top of microgrooves under a large cutting depth for the 40° tool angle, but the plastic deformation resistance of larger cutting tools performs much better than the 25.5° tool angle. For the 90° diamond tool, the burrs on the tops of microgrooves completely disappear under all cutting depths as shown in Fig. 9g, h, i. Furthermore, there is no deformation on the tops of microgrooves at all. So, the effect of cutting depth on the quality of microgrooves is not obvious for a large tool angle.

Increasing the cutting depth processing means reducing the number of cutting times, therefore improving the machining efficiency. However, increasing the cutting depth does not facilitate the removal of burrs during the machining process. Especially for small tool angles, the effect is more serious. In addition, with larger cutting depth and increase in the volume of material removal for each cutting step, the friction between the microgroove surface and the chip material greatly increases, which leads to more serious deformation at the thinner tops of grooves. So, the cutting depth should be chosen a low level (2 μm) for small tool angles. For bigger angle second-order microgrooves, it can be increased the cutting depth to improve the efficiency of the machining process.

Because the quality of microgrooves machined by a small tool angle are more sensitive to the cutting conditions, the analysis of second-order microgrooves will be focused on the 25.5° tool angle in the next experiments.

3.3 The effect of revolution speed of spindle

The cutting experiments were carried out under group 2. The revolution speed of the spindle was varied from 2000 to 6000 rpm. Since a smaller value of tool angle is sensitive to the cutting factor, a tool angle of 25.5° was used. The other

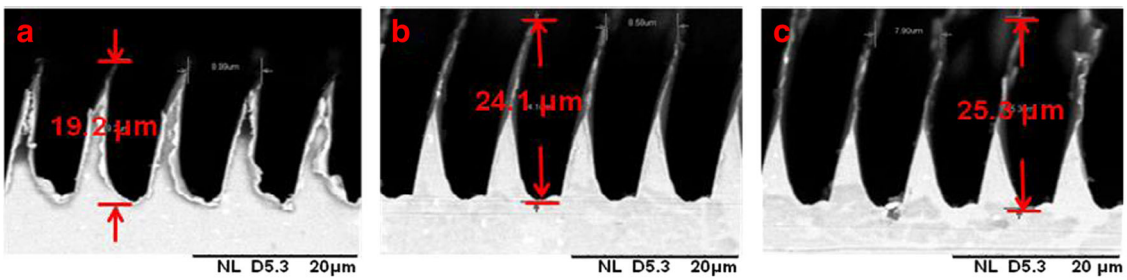

Fig. 11 The SEM of microtexture machined by UPRM at different feed rate f for tool angle 25.5°: **a** f=50 mm/min, **b** f=100 mm/min, and **c** f=200 mm/min

parameters were held constant, and the cutting depth chosen was 2 μm, and the feed rate was set at 50 mm/min.

SEM micrographs of the microgrooves machined at different revolution speeds of the spindle are shown in Fig. 10. As shown in Fig. 10a, the depth of the microgroove *d* is about 28.3 μm, which is much deeper than the set value of 20 μm and means that the cutting is not sufficient under this low revolution speed of the spindle. The phenomenon of burrs on the tops of microgrooves is obvious. The microgrooves bent in the opposite direction to the raster. The microgrooves produced at the revolution speed of the spindle of 4000 rpm are shown in Fig. 10b. The depth of microgroove is about 20.2 μm, which is very close to the set *d* value of microgroove depth; there are no burrs on the top. In addition, the microgrooves also bent toward the raster direction. Figure 10c shows the SEM photo of microgrooves machined at the revolution speed of the spindle of 6000 rpm. The depth of microgrooves is about 19.3 μm. Although the depth of second-order microgrooves is close to the theoretical value, plastic deformation extends to the middle part of microstructures where the microgrooves are relatively thicker.

Increasing the revolution speed of the spindle is beneficial for removing burrs, thus improving the second-order microgroove quality. However, the cutting tool pressure on the surface of the microgrooves also increases as well as the increase of the revolution speed of the spindle. For the microgrooves machined by a small tool angle in UPRM, the plastic deformation may extend to the position where the wall is relatively thicker. So, the revolution speed of spindle should be set within a reasonable range which should be the middle speed level speed, and the experimental works suggest that the revolution speed of spindle should be about 4000 rpm.

3.4 The effect of feed rate

The cutting experiments were carried out under group 3. Feed rate is one of the important cutting factors in UPRM. A large feed rate could greatly save machining time, but increasing the feed rate may decrease the quality of microgrooves. The other cutting parameters were fixed. The cutting depth chosen was 2 μm, and the revolution the speed of spindle was set at 4000 rpm.

The quality of second-order microgrooves is also greatly affected by the feed rate. In Fig. 11, it is found that the highest quality of microgrooves was achieved at the lowest feed rate of 50 mm/min. The depth of the microgrooves is 19.2 μm. High-quality microgrooves were obtained under a low feed rate. The top of the groove area still slightly bent in the opposite raster direction, as shown in Fig. 11a. The SEM micrograph of microgrooves machined at the feed rate of 100 mm/min is shown in Fig. 11b. Machining burrs on the top are obvious, and the depth of the microgrooves is 24.1 μm. The geometry of the second-order microgrooves machined at the feed rate of 200 mm/min is shown in Fig. 11c. The phenomenon of burrs becomes more serious, and the depth of groove is greater than 25.3 μm.

The feed rate value is another critical cutting factor that affects the quality of second-order microgrooves. Increasing the feed rate does not facilitate the removal of burrs for small tool angle cutting, so the feed rate should be controlled below a reasonable value to avoid insufficient cutting. A low level feed rate of the 50 mm/min should be chosen to machine the second-order microstrutures.

4 Conclusion

Machining grooves on ultra-precision machines is commonplace. This paper demonstrates that complex microhierarchical ribs with tiny small grooves imposed on the top used for microheat exchangers can be machined successfully in a single machining step by ultra-precision raster milling.

A series of cutting experiments was carried out to study the artificial roughness under different cutting strategies and cutting parameters on copper alloy. The results greatly contribute to the determination of fine cutting conditions and cutting strategy in ultra-precision raster milling. The cutting strategy determines the topology of artificial roughness that is produced in hierarchical ribs. The cutting depth, revolution speed of the spindle, and feed rate are found to be critical factors affecting the quality of second-order microgrooves. As the cutting depth and feed rate increase, the accuracy of microgrooves decreases with the formation of more burrs and debris. As the revolution speed of the spindle increases, machining burrs decrease, but if the revolution speed of the spindle is too high, the plastic distortion of the microgrooves becomes more pronounced.

Acknowledgments The authors would like to express their great thanks to the Research Grants Council of the Hong Kong Special Administrative Region, China (Project No. e.g., PolyU 500107)

References

1. Bergles AE, Rohsenow WM, Hartnett JP, Ganie E (1985) Techniques to augment heat transfer. Handbook of heat transfer application. McGraw Hill, New York
2. Bergles AE (1988) Some perspective on enhanced heat transfer—second-generation heat transfer technology. J Heat Transf 110(4): 1082–1096
3. Webb RL, Kim NH (2005) Principles of enhanced heat transfer, 2nd edn. Taylor & Francis, New York
4. Jaber HM, Webb RL, Stryker P (1991) Experimental investigation of enhanced tubes for steam condensers in National Heat Transfer Conference. July, 1–8
5. Karwa R, Solanki SC, Saini JS (2001) Thermo-hydraulic performance of solar air heaters having integral chamfered rib roughness on absorber plates. Energy 26(2):161–176

6. Sunden B, Xie G (2010) Gas turbine blade tip heat transfer and cooling: a literature survey. Heat Transfer Eng 31(7):527–554
7. Thianpong C, Chompookham T, Skullong S, Promvonge P (2009) Thermal characterization of turbulent flow in a channel with isosceles triangular ribs. Int Commun Heat Mass 36(7):712–717
8. Wang HT, Lee WB, Chan J, To S (2015) Numerical and experimental analysis of heat transfer in turbulent flow channels with two-dimensional ribs. Appl Therm Eng 75:623–634
9. Lee SW, Shin HS, Chu CN (2013) Fabrication of micro-pin array with high aspect ratio on stainless steel using nanosecond laser beam machining. Appl Surf Sci 264(1):653–663
10. Huang H, Li Y, Shen JY, Zhu HM, Xu XP (2002) Micro-structure detection of a gloss gray granite surface machined by the grinding process. J Mater Process Technol 129(1–3):403–407
11. Zeng YB, Yu Q, Wang SH, Zhu D (2012) Enhancement of mass transport in micro wire electrochemical machining. Ann CIRP 61(1):195–198
12. Tang Y, Chi Y, Wan ZP, Liu XK, Chen JC, Deng XX, Liu L (2008) A novel finned micro-groove array structure and forming process. J Mater Process Technol 203:548–553
13. Lee WB, Cheung CF (2001) A dynamic surface topography model for the prediction of nano-surface generation in ultra-precision machining. Int J Mech Sci 43:961–991
14. Draghici G, Paltinea C (1974) Calculation by convex mathematical programming of the optimum cutting condition when cylindrical milling. Int J Mach Tools Manuf 14(2):143–160
15. Lim EEM, Menq CH (1997) Integrated planning for precision machining of complex surfaces. Part 1. Cutting-path and feed rate optimization. Int J Mach Tools Manuf 37:61–75
16. Ramos AM, Relvas C, Simões JA (2003) The influence of finishing milling strategies on texture, roughness and dimensional deviations on the machining of complex surfaces. J Mater Process Technol 136(1–3):209–213
17. Kong LB, Cheung CF, To S, Lee WB (2009) An investigation into surface generation in ultra-precision raster milling. J Mater Process Technol 209:4178–4185
18. Cheng MN, Cheung CF, Lee WB, To S, Kong LB (2008) Theoretical and experimental analysis of nano-surface generation in ultra-precision raster milling. Int J Mach Tools Manuf 48:1090–1102
19. Duong TH, Kim HC, Lee DY, Lee SW, Park ES, Je TJ (2013) A theoretical deformation prediction of micro channels in ultra-precision machining. Int J Precis Eng Manuf 14(2):173–181
20. Zhang SJ, To S (2013) A theoretical and experimental study of surface generation under spindle vibration in ultra-precision raster milling. Int J Mach Tools Manuf 75:36–45
21. Albertelli P, Cau N, Bianchi G, Monno M (2012) The effects of dynamic interaction between machine tool subsystems on cutting process stability. Int J Adv Manuf Technol 58(9):923–932
22. Wang SJ, To S, Chen X, Chen XD, Ouyang XB (2014) An integrated optimization of cutting parameters and tool path generation in ultra-precision raster milling. Int J Adv Manuf Technol 75(9–12): 1711–1721
23. Gao HM, Fang FZ, Zhou XD (2014) Reverse analysis on the geometric errors of ultra-precision machines. Int J Adv Manuf Technol 73:1615–1624
24. Nikuradse J (1933) Laws of flow in rough pipes. Strömungsgesetze in rauhen Rohren (Translation). VDI-Forschungsheft 361. Beilage zu "Forschung auf dem Gebiete des Ingenieurwesens" Ausgabe B Band 4.